RSC Advances

ROYAL SOCIETY OF CHEMISTRY

www.rsc.org/advances

ARTICLE TYPE www.rsc.org/xxxxxx | XXXXXXXX

Design and fabrication of graphene/carbon nanotubes/activated carbon hybrid and its application for capacitive deionization

Guang Zhu*, Wenqi Wang, Xuelian Li, Jun Zhu, Hongyan Wang, Li Zhang*

Received (in XXX, XXX) Xth XXXXXXXXX 200X, Accepted Xth XXXXXXXXX 200X
First published on the web Xth XXXXXXXXX 200X
DOI: 10.1039/b000000x

In this work, graphene/carbon nanotubes (CNTs)/activated carbon (AC) (GTAC) hybrids were designed and fabricated by combing graphene, CNTs with AC into one new type of hybrid and applied as capacitive deionization (CDI) electrodes. The morphology, structure and electrochemical performance of the GTAC were characterized by scanning electron microscopy, nitrogen adsorption-desorption, cyclic voltammetry and electrochemical impedance spectroscopy. The results show that the GTAC with 72 wt% CNTs, 8 wt% graphene and 20 wt% AC exhibits the best electrochemical performance among all the samples. When used as CDI electrode, GTAC exhibits a higher electrosorption capacity of 2.30 mg g^{-1} than those of optimized graphene/AC (1.10 mg g^{-1}), graphene/CNTs (1.06 mg g^{-1}) and CNTs/AC (0.96 mg g^{-1}) in this work. The higher electrosorption capacity of GTAC can be ascribed to the superiority of the "plane-to-line-to-point" (graphene-to-CNTs-to-AC) conducting network. This result demonstrates that GTAC should be a promising candidate as CDI electrode.

1. Introduction

Capacitive deionization (CDI), also called electrosorption, is an energy-effective, low-pressure, non-membrane purification technology.[1-7] It is an electrochemical process that operates by adsorbing ions in the double layer formed at the electrodes by the application of a potential difference.[8-12] Therefore, ion adsorption capacity of a CDI electrode is directly related to its surface area and bulk conductivity. Recent advances in CDI electrode materials have been focus on development of carbon materials with novel nanostructures. Nanostructured carbon materials such as carbon aerogels (CAs),[13-15] activated carbon (AC),[16-18] carbon nanotubes (CNTs),[19-21] carbon nanofibers (CNFs),[22-25] mesoporous carbon (MC),[26-29] carbon sphere[30] and graphene[31-35] have been reported to be widely studied and explored in CDI. However, these single component carbon materials suffer problems such as low electrosorption capacity, poor wettability or poor mechanical stability, which does harm their practical applications in CDI.

To address this vitally important problem, a hierarchical nanostructure that comprises various types of carbons such as graphene, AC and CNTs with different structural dimensions and/or porous structures has been proved to greatly improve CDI performance through the structure promoted synergistic effects. For example, Shi et al. fabricated CNTs/AC composite by ball milling method.[36] Such composite composed of zero-dimensional (0D) AC and one-dimensional (1D) CNTs exhibited better CDI performance as compared to pure CNTs or AC electrodes. In another work, Li et al. fabricated graphene/AC composite by inserting 0D AC between two-dimensional (2D) graphene sheets,[37] and the obtained composite showed a higher electrosorption capacity than that of pure AC materials, demonstrating that AC particles could serve as "spacers" between graphene sheets to form a "plane-to-point" (graphene-to-AC) conducting network. Recently, 1D CNTs was used to combine with 2D graphene to obtain a "palne-to-line" (graphene-to-CNTs) sandwich structure.[38, 39] The hybrid composite showed a higher electrosorption capacity than that of CNTs. In these studies, efforts are made to integrate the advantages of two kinds of carbon materials into one new type of three-dimensional (3D) conducting network, including "line-to-point", "plane-to-point" and "plane-to-line", to improve the CDI performance. There is no denying the fact that the electrosorption capacities of these hybrid materials have been enhanced, due to the formation of 3D conducting network. Although these hybrids show an enhanced performance as compared with single component carbon, and further efforts are still needed to seek a new hybrid material with a high electrosorption capacity for practical applications of CDI.

In this work, graphene/CNTs/AC (GTAC) hybrids were designed and fabricated by combing 2D graphene, 1D CNTs with 0D AC into one new type of hybrid. This hierarchical nanostructure is composed of a "plane-to-line-to-point" (graphene-to-CNTs-to-AC) conducting network. The CDI performance of GTAC-based electrodes was further investigated and compared with graphene/AC, graphene/CNTs and CNTs/AC based electrodes. The results indicate that due to the synergistic effects of graphene, CNTs and AC, GTAC with 72 wt% CNTs, 8 wt% graphene and 20 wt% AC exhibits the best electrochemical performance among all the samples.

2. Experimental

2.1 Preparation of samples

Graphene oxide (GO) was prepared according to the method reported in literature.[40] CNTs purchased from Nanotech Port Co. Ltd. (Shenzhen, China) and AC was immersed in 1 M nitric acid for at least 4.5 hours.

Preparation of graphene/AC. Typically, a certain amount of GO solution was put into 200 ml oxidized AC solution under stirring for 8 hours. The mixture was placed in a chemical bath at a temperature of 35 ^{o}C, and then hydrazine was carefully dropped into the solution until the pH value reached 7. Meanwhile, the color of the solution changed from light

yellow to black, indicating that the reduction was complete. Finally, the mixture was left overnight and then filtered. The final product was dried in a vacuum oven at 60 °C. The ratio of GO and AC was changed. After a series of tests (see Fig. 1a), the optimized weight ratio of GO and AC is 1:9.

Preparation of graphene/CNTs. The preparation process of graphene/CNTs is similar to that of graphene/AC. After a series of tests (see Fig. 1b), the optimized weight ratio of GO and CNTs is 1:9.

Preparation of CNTs/AC. The preparation process of CNTs/AC is similar to that of graphene/AC. After a series of tests (see Fig. 1c), the optimized weight ratio of CNTs and AC is 1:9.

Preparation of GTAC. GTAC was prepared by using optimized GO/CNTs mixed solution and AC solution as precursors. The preparation process is similar to that of graphene/AC. By changing the content of AC, a set of GTAC samples were obtained. The as-prepared GTAC samples with 10, 20 and 30 wt% AC were named GTAC-10, GTAC-20 and GTAC-30, respectively.

2.2 Characterization

The surface morphology and structure of the samples were examined by field emission scanning electron microscopy (FESEM, HATICH S4800) and JEOL-2010 high-resolution transmission electron microscope (HRTEM). Nitrogen adsorption-desorption isotherms were measured at 77 K with an ASAP 2020 Accelerated Surface Area and Porosimetry System (Micrometitics, Norcross, GA). X-ray photoelectron spectroscopy (XPS) measurements were performed on an Imaging Photoelectron Spectrometer (Axis Ultra, Kratos Analytical Ltd.) with a monochromatic Al Ka X-ray source. The potential sweep cyclic voltammetry (CV) and electrochemical impedance spectroscopy (EIS) measurements were carried out in 1 M NaCl solution by using Autolab PGSTAT 302N electrochemical workstation in a three-electrode mode, including a standard calomel electrode as reference electrode and a platinum foil as counter electrode. In the EIS measurement, a frequency range of 0.1 Hz to 100 kHz and an AC amplitude of 5 mV were applied. The specific capacitance can be obtained from CV curves using the following equation:

$$C = \tilde{i}/(v \times m) \quad (1)$$

where $\tilde{i}$ is the average current (A), v is the scan rate (V s^{-1}) and m is the mass of electrodes (g).

2.3 Electrosorption experiments

The electrodes were prepared by mixing 80 wt% of samples, 10 wt% of acetylene black, and 10 wt% of polyvinyl alcohol slurry. The mixtures were pressed onto graphite papers and dried in vacuum oven at 60 °C overnight.

The CDI experiments were investigated by batch-mode electrosorption experiments with a continuously recycling system. In each experiment, the analytical NaCl was employed as the target solution with a volume of 50 mL and the flow rate was 27 mL/min. A direct voltage of 1.2 V was applied. The initial conductivity of NaCl solution was ~100 μS cm^{-1}, and the atmosphere temperature was kept at 298 K. The relationship between conductivity and concentration was obtained according to a calibration table made prior to the experiment.[41] The concentration variation was continuously monitored and measured at the outlet of the unit cell by using an ion conductivity meter.

In our experiment, the electrosorption capacity (Γ, mg g^{-1}) was defined as follows:

$$\Gamma = \frac{(C_0 - C_e) \times V}{m} \quad (2)$$

where C_0 is initial NaCl concentration (mg L^{-1}), C_e is the final NaCl concentration (mg L^{-1}), V is the volume of NaCl solution (L) and m is the mass of electrodes (g).

Charge efficiency (Λ)[42-44] is a functional tool to gain insight into the double layer formed at the interface between the electrode and solution, as calculated according to the following equation:

$$\Lambda = \frac{\Gamma \times F}{\Sigma} \quad (3)$$

where F is the Faraday constant (96485 C mol^{-1}), Γ is the electrosorption capacity (mol g^{-1}) and Σ (charge, C g^{-1}) is obtained by integrating the corresponding current.

3. Results and discussion

3.1 Ratio optimization of graphene/AC, graphene/CNTs and CNTs/AC

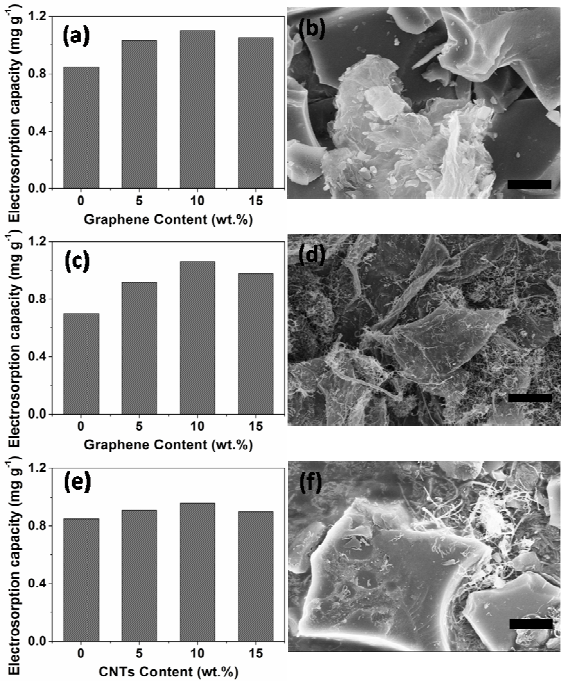

Fig. 1 (a, c, e) The electrosorption capacities of (a) graphene/AC, (c) graphene/CNTs and (e) CNTs/AC hybrids. (b, d, f) The SEM images of (b) graphene/AC, (d) graphene/CNTs and (f) CNTs/AC hybrids with an optimized weight ratio. (Scale bar : 2 μm). All CDI tests are conducted in NaCl solution with a volume of 50 mL and an initial conductivity of ~100 μS cm^{-1}. The applied voltage is 1.2 V.

Fig. 1(a) shows the electrosorption capacities of graphene/AC-based CDI electrodes obtained from the optimizing tests. Clearly, when the weight ratio of GO and AC is 1:9, the corresponding CDI performance is the best, indicating that the optimized weight ratio of GO and AC in graphene/AC is 1:9. Furthermore, the corresponding SEM image is shown in Fig. 1(b). Graphene displays a transparent and layered structure, and serves as a bridge between AC particles.

Fig. 1(c) shows the electrosorption capacities of graphene/CNTs-based CDI electrodes obtained from the optimizing tests. Clearly, when the weight ratio of GO and CNTs is 1:9, the corresponding CDI performance is the best, indicating that the optimized weight ratio of GO and CNTs in graphene/CNTs is 1:9. Furthermore, the corresponding SEM image is shown in Fig. 1(d). It can be seen that CNTs and graphene are relatively uniformly dispersed, and form a "plane-to-line" (graphene-to-CNTs) porous structure.

Fig. 1(e) shows the electrosorption capacities of CNTs/AC-based CDI electrodes obtained from the optimizing tests. Clearly, when the weight ratio of CNTs and AC is 1:9, the corresponding CDI performance is the best, indicating that the optimized weight ratio of CNTs and AC in CNTs/AC is 1:9. Furthermore, the corresponding SEM image is shown in Fig. 1(f). It can be seen that CNTs exist between AC particles, which can help bridge between the adjacent AC particles, thus improving the electrical conductivity of the hybrid.

3.2 Characterization

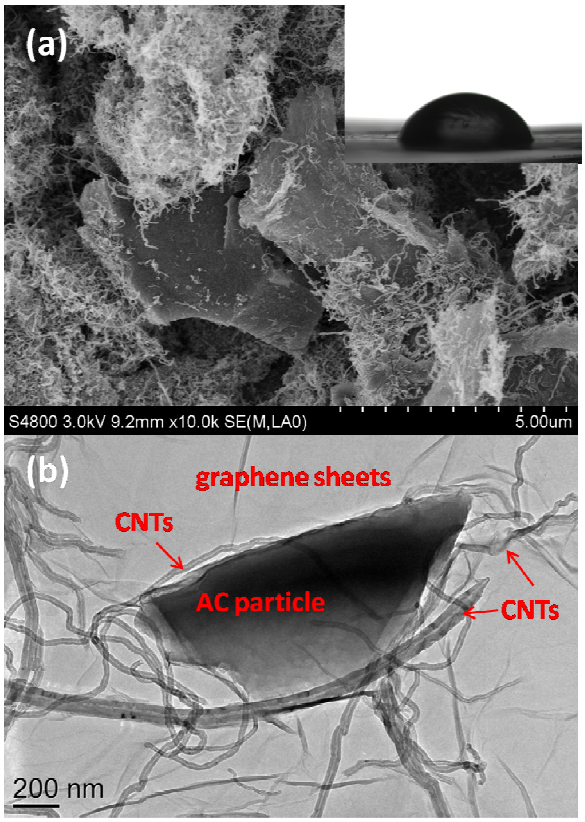

Fig. 2 SEM image (a) and TEM image (b) GTAC-20. Inset of (a) is the contact angle image.

Fig. 2 describes the morphology and structure of GTAC-20. As shown in SEM image (Fig. 2(a)), the GTAC shows a hierarchical porous structure with AC particles inserting between CNTs and graphene, which will decrease the aggregation of graphene and help improve the surface area of the composite as well as provides many more available spaces to accommodate ions during electrosorption. On the other hand, with AC employed into the composite, the GTAC forms a "plane-to-line-to-point" (graphene-to-CNTs-to-AC) conducting network, which can facilitate rapid transport of the electrolyte ions within the electrode materials and thus improve the electrosorption capacity of GTAC. The contact angel of such hybrid is 65 º (Inset of Fig. 2(a), indicating that GTAC-20 should have a good wettability. Furthermore, the corresponding TEM image of GTAC-20 is shown in Fig. 2(b). Obviously, both graphene and CNTs are relatively uniformly dispersed around AC particles, thus constituting the novel "plane-to-line-to-point" (graphene-to-CNTs-to-AC) conducting network.

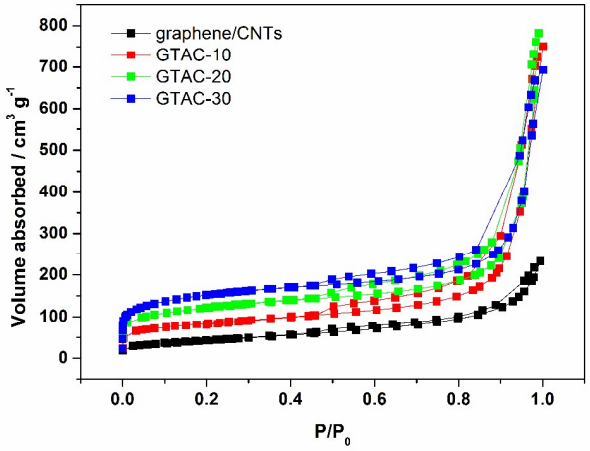

Fig. 3 Nitrogen adsorption–desorption isotherms of graphene/CNTs, GTAC-10, GTAC-20 and GTAC-30.

Table 1 Textural property of samples.

Sample	a_{total} (m^2 g^{-1})	V_{total} (cm^3 g^{-1})	a_{micro} (m^2 g^{-1})	a_{micro}/ a_{total}	$Pore_{ave}$ (nm)
graphehe/CNTs	151.26	0.34	—	—	9.08
GTAC-10	287.34	1.03	167.13	0.58	14.40
GTAC-20	426.56	1.19	166.04	0.39	11.39
GTAC-30	520.94	0.98	283.47	0.54	7.50

The specific surface area is characterized by N_2 adsorption–desorption isotherms. Fig. 3 displays the N_2 adsorption–desorption isotherms of graphene/CNTs and GTAC. Both graphene/CNTs and GTAC show a typical type IV hysteresis loop as defined by IUPAC, which is characteristic of mesoporous materials.[39, 45] The hysteresis loop which appears at lower relative pressure (0.4–0.8) indicates the presence of mesopores and at higher relative pressure (0.8–1.0) is attributed to macropores.[45] The specific surface areas, pore volumes and mean pore diameters of all samples are shown in Table 1. It can be seen that all GTAC samples show a higher specific surface area and larger pore volume than graphene/CNTs. Moreover, with the increase in AC content,

the specific surface area of GTAC increases. This phenomenon can be ascribed as follows: 1) with the introduction of AC, the aggregation of graphene or CNTs can be further alleviated, and thus more pores can be generated, which help improve the surface area and pore volume of GTAC; 2) with the further increase in AC content, the surface area of GTAC-30 increases due to the increase of high-surface-area AC. Conversely, the pore volume of GTAC-30 decreases due to the low pore volume of AC. In addition, GTAC-20 exhibits the lowest a_{micro}/a_{total} ratio (0.39) among all GTAC samples, indicating the highest mesoporous ratio of GTAC-20. The higher mesoporous ratio in porous carbon will lead in a higher electrosorption capacity.[46] Therefore, GTAC-20 is expected to possess the highest electrosorption capacity among all samples.

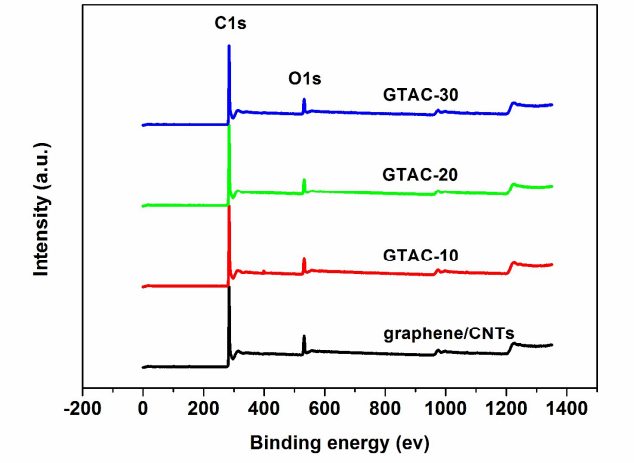

Fig. 4 XPS spectra of graphene/CNTs and GTACs.

The oxygen contents of graphene/CNTs and GTACs are tested by XPS spectra, as shown in Fig. 4. Clearly, all samples show only the presence of C1s and O1s peaks at about 284 and 533 eV with low contents of oxygen element (7.1-9.4 at.%), indicating that GO in these samples has been reduced to graphene effectively after annealing.

3.3 Electrochemical analysis

Fig. 5(a) shows the CV curves of graphene/CNTs and GTACs electrodes at a scan rate of 5 mV s^{-1} in 1 M NaCl solution. It is found that no significant Faradaic reaction is observed for any electrode, illustrating that ions are adsorbed on the electrode surface by forming an electric double layer due to Coulombic interaction rather than electrochemical reaction.[47] The specific capacitances of GTAC-10, GTAC–20 and GTAC-30 are 64 F g^{-1}, 93.5 F g^{-1} and 76.5 F g^{-1}, respectively, which are all higher than that of GS/CNTs (56 F g^{-1}). Furthermore, GTAC-20 shows the highest specific capacitance, indicating the GTAC-20 should be a promising candidate as CDI electrode materials. These results should be attributed to the following reasons: i) the introduction of AC should be beneficial for increasing specific surface area and pore volume, and impoving "plane-to-line-to-point" (graphene-to-CNTs-to-AC) conducting network of the GTAC, and thus help to improve the capacitance of GTAC; ii) besides the specific surface area and pore volume, mesoporous ratio in porous carbon also plays an important role in determining the electrosorption capacity.[46] Therefore, although the total specific surface area of the GTAC-20 is not the largest, due to the highest mesoporous ratio of GTAC-20, it shows the highest specific capacitance. Fig. 5(b) displays the specific capacitances of graphene/CNTs and GTACs electrodes at different scan rates. Obviously, the GTAC-20 has the highest specific capacitance at all scan rates, suggesting that there is an intimate contact between the electrolyte and the active material. Thus, the GTAC-20 was selected as electrode material for CDI experiment.

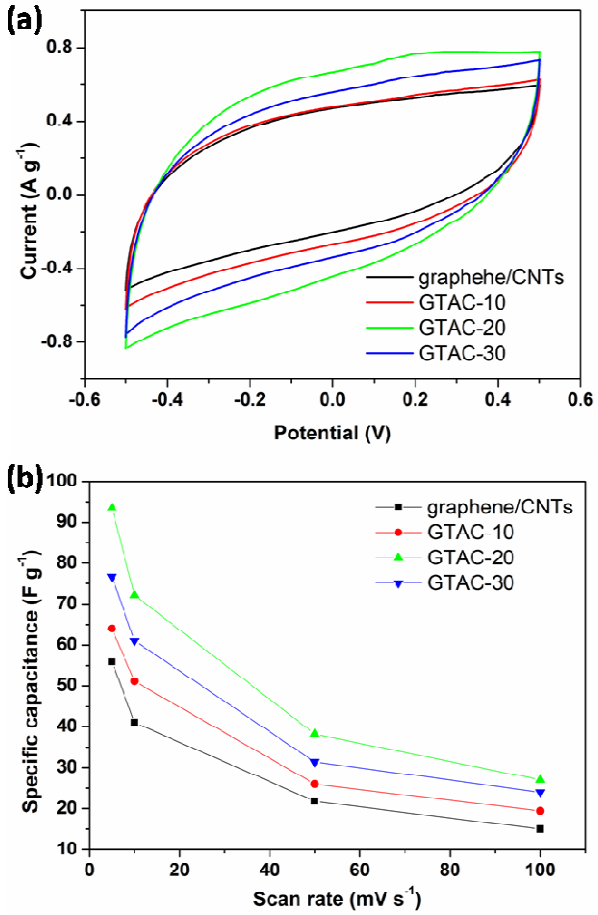

Fig. 5 CV curves of the graphene/CNTs and GTACs electrodes at a scan rate of 5 mV s^{-1} (a) and the specific capacitances of the electrodes vs. scan rates (b). All the profiles were obtained in a 1 M NaCl aqueous solution.

EIS analysis has been recognized as one of the principal methods to examine the electrical conductivity of a carbon electrode. The Nyquist profiles of the GTAC-20 and GS/CNTs electrodes in a 1 M NaCl aqueous solution are presented in Fig. 6. It can be obviously seen that the plots display similar shapes, consisting of a linear trait at the low frequency region and a small quasi-semicircle at the high frequency one. The small quasi-semicircle at the high-frequency region is derived from the double layer capacitance (C_{dl}) in parallel with the charge transfer resistance (R_{ct}).[39] The R_{ct} can be obtained from the diameter of the semicircle. The value for GTAC-20 is around 0.78 Ω, much lower than that of

graphene/CNTs (1.1 Ω), indicating that GTAC-20 should have a lower charge-transfer resistance and a superb conductivity.

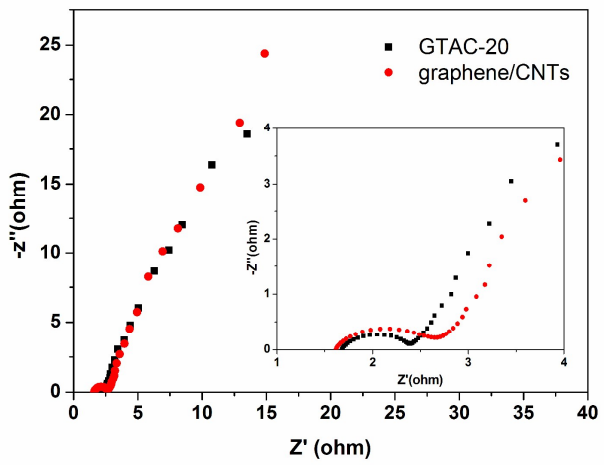

Fig. 6 Nyquist plots of the GTAC-20 and graphene/CNTs. Inset shows the expanded high-frequency region of the plots.

3.4 CDI tests

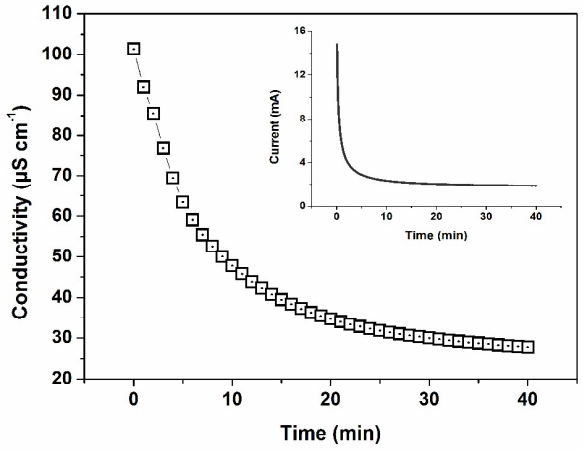

Fig. 7 The typical conductivity for GTAC-20 electrodes over 40 minutes in NaCl solution with an initial conductivity of ~100 μS cm^{-1} at an applied voltage of 1.2 V. Inset is corresponding current transient.

To determine the electrosorption performance of GTAC-20 electrodes, batch mode CDI experiment was carried out in NaCl solution with an initial conductivity of ~100 μS cm^{-1} at an applied potential of 1.2 V. The current variation was recorded simultaneously and independently at each experiment. Clearly, once the electric field was applied, the adsorption amount increased sharply. Then, the change became gradually lower until equilibrium was reached. As calculated, the electrosorption capacity and charge efficiency of GTAC-20 is 2.30 mg g^{-1} and 0.53, respectively. Notably, the value of 2.30 mg g^{-1} for GTAC-20-based CDI electrodes is much higher than those for the optimized graphene/AC (1.10 mg g^{-1}), graphene/CNTs (1.06 mg g^{-1}) and CNTs/AC (0.96 mg g^{-1}) in this work. Moreover, this value is also higher than those of graphene-based electrodes reported in the literatures (0.27–2.0 mg g^{-1}).[26, 31, 35-38] The higher electrosorption capacity of GTAC-20 can be ascribed to the novel "plane-to-line-to-point" (graphene-to-CNTs-to-AC) conducting network in GTAC-20.

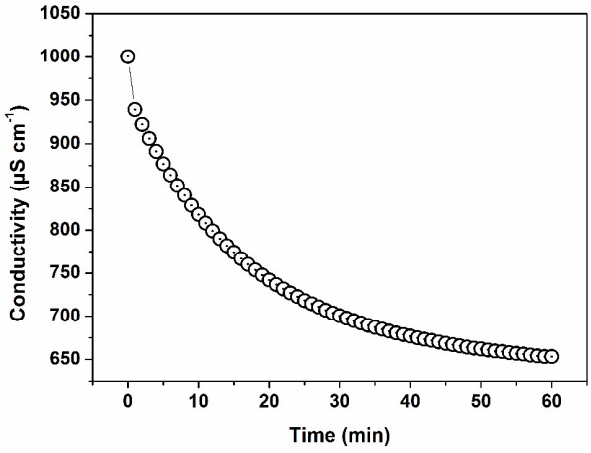

Fig. 8 The typical conductivity for GTAC-20 electrodes in NaCl solution with an initial conductivity of ~1000 μS cm^{-1} at an applied voltage of 1.2 V.

In order to get a better understanding of the superiority of the novel "plane-to-line-to-point" conducting network in GTAC-20. The electrosorption experiments using GTAC-based CDI electrodes were performed in NaCl solution with an initial conductivity of ~1000 μS cm^{-1} at an applied voltage of 1.2 V (Fig. 8). The electrosorption capacity of GTAC-20 is calculated to be 10.94 mg g^{-1}, which is amongst the highest values reported so far for porous carbon.[1, 40, 43, 48, 49]

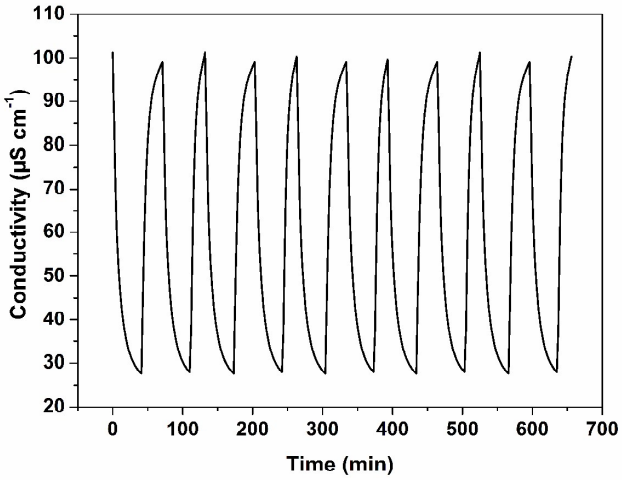

Fig. 9 Recycle electrosorption experiment for the GTAC-20 electrode.

To investigate the recycle of electrosorption process of the GTAC-20, repeating charge-discharge experiment using GTAC-20 electrode was carried out. The initial solution conductivity is 100 μS cm^{-1}. When the conductivity gets back to the initial value in the first discharge process the second charge process starts. Fig. 9 shows the conductivity transient over 10 charge-discharge cycles. Obviously, the repeatability of electrosorption process can be realized in this unit cell. In the practical experiment, electrosorption capacity declination has not been observed in this unit cell after over 30 charge-discharge experiments.

4. Conclusions

In this work, GTAC composites were prepared via a facile chemical approach, and investigated as CDI electrode for the first time. The results show that (i) the GTAC-20 has the highest specific capacitance among these GTAC composites; (ii) the GTAC-20 shows a higher electrosorption capacity of 2.30 mg g^{-1} at an applied potential of 1.2 V than those of optimized graphene/AC (1.10 mg g^{-1}), graphene/CNTs (1.06 mg g^{-1}) and CNTs/AC (0.96 mg g^{-1}) in this work; (iii) the enhanced electrosorption performance of the GTAC-20 is ascribed to the novel "plane-to-line-to-point" (graphene-to-CNTs-to-AC) conducting network in GTAC-20; (iv) the GTAC-20 should be a promising candidate as electrode material for CDI.

Acknowledgment

This work is supported by the National Science Foundation of China (NSFC) (21271136), the Provincial Natural Science Foundation of Anhui (1508085ME104 and 1408085MB40), the Scientific Research Foundation for the Anhui Provincial Returned Overseas Chinese Scholars (Electrospun low dimensional TiO_2 nano-structures and application in photovoltaic devices), the Key Program of Outstanding Youth Talents in Higher Education Institution (GXYQZD2016343 and GXFXZD2016258), the Program of Innovative Research Team of Anhui Provincial Education Department (Photoelectric information materials and new energy devices), the Important Project of Anhui Provincial Education Department (KJ2015A250 and KJ2013Z315), the Scientific Research Foundation of Suzhou University (2014XQNRL012，2012YKF02 and 2014XJGG01), and the Program of Innovative Research Team of Suzhou University (2013kytd02).

Notes and references

Anhui Key Laboratory of Spin Electron and Nanomaterials, Suzhou University, Suzhou 234000, P. R. China, Tel.: +86-557-2871006; Fax: +86-557-2871003; E-mail: Prof. L. Zhang zhlisuzh@163.com; Prof. G. Zhu guangzhu@ahsztc.edu.cn.

1. H. Yin, S. Zhao, J. Wan, H. Tang, L. Chang, L. He, H. Zhao, Y. Gao and Z. Tang, *Adv. Mater.* , 2013, **25**, 6270-6276.
2. M. E. Suss, P. Biesheuvel, T. F. Baumann, M. Stadermann and J. G. Santiago, *Environ Sci Technol*, 2014.
3. C. HeeáCho, M. HeeáHan and D. KookáKim, *Energy Environ. Sci.*, 2013, **6**, 1471-1475.
4. H. Wang, D. Zhang, T. Yan, X. Wen, J. Zhang, L. Shi and Q. Zhong, *J. Mater. Chem. A*, 2013, **1**, 11778-11789.
5. P. Hojati-Talemi, L. Zou, M. Fabretto and R. D. Short, *Electrochim. Acta*, 2013, **106**, 494-499.
6. H. Wang, L. Shi, T. Yan, J. Zhang, Q. Zhong and D. Zhang, *J. Mater. Chem. A*, 2014, **2**, 4739-4750.
7. Z. Peng, D. Zhang, L. Shi and T. Yan, *J. Mater. Chem.*, 2012, **22**, 6603-6612.
8. E. Garcia-Quismondo, C. Santos, J. Lado, J. Palma and M. A. Anderson, *Environ. Sci. Technol.*, 2013, **47**, 11866-11872.
9. Y. Liu, L. Pan, X. Xu, T. Lu, Z. Sun and D. H. Chua, *Electrochim. Acta*, 2014, **130**, 619-624.
10. X. Gao, A. Omosebi, J. Landon and K. Liu, *Electrochem. Commun.*, 2014, **39**, 22-25.
11. M. T. Z. Myint, S. H. Al-Harthi and J. Dutta, *Desalination*, 2014, **344**, 236-242.
12. X. Xu, L. Pan, Y. Liu, T. Lu and Z. Sun, *J. Colloid Interface Sci.*, 2015, **445**, 143-150.
13. Y. Liu, C. Nie, L. Pan, X. Xu, Z. Sun and D. H. Chua, *Inorg. Chem. Front.*, 2014, **1**, 249-255.
14. P. Xu, J. E. Drewes, D. Heil and G. Wang, *Water Res.*, 2008, **42**, 2605-2617.
15. J. C. Farmer, D. V. Fix, G. V. Mack, R. W. Pekala and J. F. Poco, *J. Electrochem. Soc.*, 1996, **143**, 159-169.
16. S.-i. Jeon, J.-g. Yeo, S. Yang, J. Choi and D. K. Kim, *J. Mater. Chem. A*, 2014.
17. L. Zou, G. Morris and D. Qi, *Desalination*, 2008, **225**, 329-340.
18. Z. Chen, C. Song, X. Sun, H. Guo and G. Zhu, *Desalination*, 2011, **267**, 239-243.
19. L. Wang, M. Wang, Z.-H. Huang, T. Cui, X. Gui, F. Kang, K. Wang and D. Wu, *J. Mater. Chem.*, 2011, **21**, 18295-18299.
20. C. Y. Nie, L. K. Pan, Y. Liu, H. B. Li, T. Q. Chen, T. Lu and Z. Sun, *Electrochim. Acta*, 2012, **66**, 106-109.
21. Y. K. Zhan, L. K. Pan, C. Y. Nie, H. B. Li and Z. Sun, *J. Alloys Compd.*, 2011, **509**, 5667-5671.
22. G. Wang, C. Pan, L. Wang, Q. Dong, C. Yu, Z. Zhao and J. Qiu, *Electrochim. Acta*, 2012, **69**, 65-70.
23. G. Wang, Q. Dong, Z. Ling, C. Pan, C. Yu and J. Qiu, *J. Mater. Chem.*, 2012, **22**, 21819-21823.
24. A. G. El-Deen, N. A. M. Barakat, K. A. Khalil and H. Y. Kim, *J Mater. Chem. A*, 2013, **1**, 11001-11010.
25. A. G. El-Deen, N. A. Barakat, K. A. Khalil and H. Y. Kim, *New J. Chem.*, 2014, **38**, 198-205.
26. D. S. Zhang, X. R. Wen, L. Y. Shi, T. T. Yan and J. P. Zhang, *Nanoscale*, 2012, **4**, 5440-5446.
27. C. Tsouris, R. Mayes, J. Kiggans, K. Sharma, S. Yiacoumi, D. DePaoli and S. Dai, *Environ. Sci. Technol.*, 2011, **45**, 10243-10249.
28. L. Zou, L. Li, H. Song and G. Morris, *Water Res.*, 2008, **42**, 2340-2348.
29. Y.-C. Tsai and R.-a. Doong, *Synthetic Met.*, 2015, **205**, 48-57.
30. Y. Liu, L. Pan, T. Chen, X. Xu, T. Lu, Z. Sun and D. H. Chua, *Electrochim. Acta*, 2015, **151**, 489-496.
31. Z. Y. Yang, L. J. Jin, G. Q. Lu, Q. Q. Xiao, Y. X. Zhang, L. Jing, X. X. Zhang, Y. M. Yan and K. N. Sun, *Adv. Funct. Mater.*, 2014, **24**, 3917-3925.
32. H. Lei, T. Yan, H. Wang, L. Shi, J. Zhang and D. Zhang, *J. Mater. Chem. A*, 2015, **3**, 5934-5941.
33. X. Xu, Z. Sun, D. H. Chua and L. Pan, *Sci. Rep.*, 2015, **5**, 11225.
34. X. Xu, L. Pan, Y. Liu, T. Lu, Z. Sun and D. H. Chua, *Sci. Rep.*, 2015, **5**, 8458.
35. X. Xu, Y. Liu, T. Lu, Z. Sun and L. Pan, *J. Mater. Chem. A*, 2015, **3**, 13418-13425.
36. D. Zhang, L. Shi, J. Fang and K. Dai, *Mater. Lett.*, 2006, **60**, 360-363.
37. H. B. Li, L. K. Pan, C. Y. Nie, Y. Liu and Z. Sun, *J. Mater. Chem.*, 2012, **22**, 15556-15561.
38. D. Zhang, T. Yan, L. Shi, Z. Peng, X. Wen and J. Zhang, *J. Mater. Chem.*, 2012, **22**, 14696-14704.
39. H. Li, S. Liang, J. Li and L. He, *J. Mater. Chem. A*, 2013, **1**, 6335-6341.
40. X. Xu, Y. Liu, M. Wang, X. Yang, C. Zhu, T. Lu, R. Zhao and L. Pan, *Electrochim. Acta*, 2016, **188**, 406-413.
41. H. B. Li, T. Lu, L. K. Pan, Y. P. Zhang and Z. Sun, *J. Mater. Chem.*, 2009, **19**, 6773-6779.
42. S. Porada, R. Zhao, A. Van Der Wal, V. Presser and P. M. Biesheuvel, *Prog. Mater. Sci.*, 2013, **58**, 1388-1442.
43. S. Porada, L. Borchardt, M. Oschatz, M. Bryjak, J. Atchison, K. Keesman, S. Kaskel, P. Biesheuvel and V. Presser, *Energy Environ. Sci.*, 2013, **6**, 3700-3712.
44. R. Zhao, P. Biesheuvel, H. Miedema, H. Bruning and A. Van der Wal, *J. Phys. Chem. Lett.*, 2009, **1**, 205-210.
45. X. Wen, D. Zhang, T. Yan, J. Zhang and L. Shi, *J. Mater. Chem. A*, 2013, **1**, 12334-12344.

46. C.-L. Yeh, H.-C. Hsi, K.-C. Li and C.-H. Hou, *Desalination*, 2015, **367**, 60-68.
47. L. Li, L. Zou, H. Song and G. Morris, *Carbon*, 2009, **47**, 775-781.
48. S. Porada, F. Schipper, M. Aslan, M. Antonietti, V. Presser and T. P. Fellinger, *ChemSusChem*, 2015, **8**, 1867-1874.
49. B. Qian, G. Wang, Z. Ling, Q. Dong, T. Wu, X. Zhang and J. Qiu, *Adv. Mater. Interfaces*, 2015, **2**, 1500372.

Graphical Contents Entry

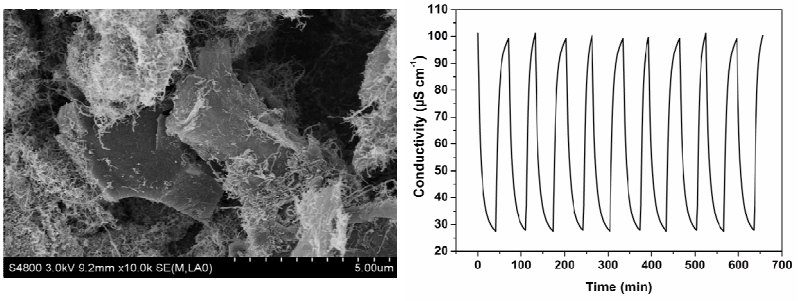

Novel three-component graphene/carbon nanotubes (CNTs)/activated carbon (AC) (GTAC) hybrids were prepared via a facile chemical approach, and investigated as capacitive deionization (CDI) electrode for the first time. As-prepared GTAC-20 hybrid exhibits a high elcetrosorption capacity of 2.30 mg g^{-1} and good repeatability, this value of 2.30 mg g^{-1} outperforms graphene/CNTs, graphene/AC and CNTs/AC based electrodes reported recently.